# Experimental observations of synchronization between two bidirectionally coupled physically dissimilar oscillators

Ke Huang [1,*] Francesco Sorrentino,[2] and Mani Hossein-Zadeh [1]

[1]*Center for High Technology Materials, The University of New Mexico, 1313 Goddard Street SE, Albuquerque, New Mexico 87106, USA*

[2]*Department of Mechanical Engineering, The University of New Mexico, Albuquerque, New Mexico 87131, USA*

(Received 14 April 2020; revised 20 August 2020; accepted 10 September 2020; published 20 October 2020)

We experimentally study the complex dynamics of two mutually coupled physically dissimilar oscillators with two different kinds of coupling mechanisms. Specifically, an optoelectronic oscillator is coupled to a Colpitts oscillator via optical power and the Colpitts oscillator is coupled back to the optoelectronic oscillator via electric voltage. We investigate and characterize phase synchronization and generalized chaos synchronization in this coupled system. Phase synchronization is observed when both oscillators are preset to oscillate periodically prior to coupling while generalized chaos synchronization is observed when both oscillators are preset to oscillate chaotically prior to coupling. In the periodical oscillation regime, we observe a linear relationship between the strengths of the two unidirectional coupling factors at which the system transitions to a synchronized state. In the chaotic regime, we observe a transition from hyperchaos to chaos associated with the onset of generalized synchronization.

DOI: 10.1103/PhysRevE.102.042215

## I. INTRODUCTION

The dynamics of coupled oscillators remains a subject of active investigation. Many theoretical papers reported important findings in the context of coupled homogeneous oscillators [1–7] and heterogeneous oscillators [8–10]. However, experimental work is needed to verify theoretical predictions against noise mechanisms, parasitic effects, and unexpected coupling mechanisms. Experimental research has considered coupled homogeneous oscillators in various domains, such as biological oscillators [11], optical oscillators [12,13], electrical oscillators [14–16], optomechanical oscillators [17], chemical oscillators [18], mechanical oscillators [19], optoelectronic oscillators [20,21], and so on. While several experimental works have dealt with coupled homogeneous oscillators, a relatively unexplored area is the study of interactions between physically dissimilar oscillators [22–24].

Instances of coupled heterogeneous oscillators may be found in many biological systems. An example is provided by the cardiorespiratory interactions between the lungs and the heart, with each having different temporal variations; the respiratory oscillation is near sinusoidal [25], while the heartbeat has a more complex behavior that may vary due to a disease or other factors. The lungs may be considered as a single oscillator [26] while the heart is composed of numerous oscillating cells [27,28]. There is scientific evidence that arrhythmia and other cardiac disorders are associated with changes in other oscillations in the body, such as neuronal and circadian [29,30].

It is therefore important to understand how physically dissimilar oscillators interact with each other and what are the possible causes for dramatic changes in their dynamics. Unfortunately, experimentation with biological systems is not easy due to the weak and irregular nature of their interactions [22] and most importantly due to the inherent difficulty of isolating the oscillating entities and quantifying their coupling. As such, experimental platforms based on nonbiological systems may provide a proxy for much more complex biologically systems and pave the way toward a better understanding of their behavior. For example, Prasad *et al.* observed a phase-flip bifurcation, or a transition from in-phase synchrony to out-of-phase synchrony as the coupling delay between two oscillators is increased in an electrical circuit [31]; later, Adhikari *et al.* observed similar transitions in neuron models involving a large number of interacting neurons [32].

Notwithstanding the prevalence of dissimilar interactions in biological and other systems, experimental work on coupled heterogeneous oscillators has been sporadic. Here, we experimentally study the complex dynamics of two physically dissimilar oscillators bidirectionally coupled using two different types of coupling mechanisms. Specifically, an optoelectronic oscillator (OEO) is coupled to a Colpitts oscillator via optical power and the Colpitts oscillator is coupled back to the OEO via electrical voltage. The OEO is a delayed-feedback nonlinear hybrid oscillator in which both optical and electrical signals flow in a single feedback loop; as such the OEO can be coupled to another oscillator both optically and electrically. Like other delayed feedback oscillators, the OEO can be configured to generate a wide variety of wave forms with differing degrees of complexity. In particular, at large optical pump power, an OEO can exhibit high dimensional chaotic behavior [33–36]. The Colpitts oscillator, which has been extensively used for investigation of various dynamical phenomena, is an electronic oscillator based on an *LC* tank.

*huangk@unm.edu

 

This oscillator can also exhibit a rich dynamical behavior including periodic oscillation, period doubling, and chaotic oscillations [37–40]. We investigate and characterize phase synchronization and generalized chaos synchronization in the coupled OEO-Colpitts system.

## II. EXPERIMENTAL ARRANGEMENT

Figure 1(a) shows the configuration of the mutually coupled OEO and Colpitts circuits, where the red line connecting the "MZM" to "Optical Atten" indicates optical coupling and the black line connecting "rf Atten" to "RF combiner" indicates electrical coupling. The parameters $\kappa_{12}$ and $\kappa_{21}$ represent the strength of the optical and electrical coupling, respectively. Figure 1(b) shows the implementation of the coupled OEO-Colpitts system used in our experiment. The OEO (oscillator system in the top shaded region) is fabricated using a simple single loop architecture with an optical delay line consisting of 1 km single mode optical fiber. The optical pump power is generated by a narrow linewidth ($\sim$0.5 MHz) fiber coupled semiconductor laser at a wavelength of 1.55 $\mu$m. After passing through a polarization controller, the pump power is fed into a Mach-Zehnder modulator (MZM) where the transmitted optical power through the MZM is a nonlinear function of the applied voltage on the rf port of the MZM. Light exiting the modulator passes through a 1-km-long single mode optical fiber and then is converted to voltage by a photodiode (PD1). The resulting voltage signal passes through an rf combiner and then amplified by an rf amplifier, the amplified signal is filtered by an rf filter and the loop is closed by feeding back the filtered signal to the rf port of the MZM. A small portion ($-19$ dB) of the rf power circulating in the OEO loop is coupled out by an rf coupler and fed to one of the four channels (channel no. 1) of an oscilloscope (OSC) (TDS2024B, Tektronix, 4 channels, 200 MHz bandwidth, 2GS/s sample rate) and an electrical spectrum analyzer (ESA) (N9320B, Keysight, 9 kHz–3 GHz range, 10 Hz–1 MHz Resolution Bandwidth) for monitoring the temporal and spectral characteristics of the OEO.

The Colpitts oscillator circuit comprises an *LC* tank and an NPN bipolar transistor configured as a common emitter amplifier. The *LC* tank consists of one inductor ($L$) and two capacitors ($C_1$ and $C_2$). A photodiode (PD2) is connected between the collector port and base port of the transistor to enable optical coupling to the Colpitts. The same oscilloscope (through channel no. 2) and electrical spectrum analyzer are used to monitor the wave form and frequency spectrum of the Colpitts from the collector port of the transistor.

In order to couple the OEO to the Colpitts oscillator, half of the circulating optical power in the OEO loop is directed to PD2 using a $1 \times 2$ 50/50 fiber optical directional coupler. The coupled optical power is converted to photocurrent by PD2 and injected to the base port of the transistor because of the bias network constructed using resistors $R_3$ and $R_4$. The photocurrent that entered the base port gets amplified in the transistor together with the Colpitts intrinsic current and then circulate inside the *LC* tank. The magnitude of the coupled optical power and so the resulting photocurrent can be adjusted by a tunable fiber optical attenuator. To couple the Colpitts oscillator to the OEO, a portion of the rf voltage from the collector port of the transistor is unidirectionally directed to the rf power combiner placed in the OEO loop using an electronic buffer and an rf power attenuator. This coupled rf voltage is combined with the OEO intrinsic rf voltage in the rf combiner and then circulates inside the OEO loop. The magnitude of the coupled rf voltage is controlled by the tunable rf attenuator. As such OEO and Colpitts are mutually coupled via two different types of coupling mechanisms (i.e., electronic and optoelectronic), where both couplings are unidirectional and adjustable.

Using the coupled system shown in Fig. 1(b) we have investigated the synchronization of the mutually coupled OEO and Colpitts oscillators in the two distinctive regimes which are (1) OEO and Colpitts both oscillate periodically before coupling, (2) OEO and Colpitts both oscillate chaotically before coupling. The values of the system parameters are adjusted (as listed in Tables I and II) to ensure that the OEO and Colpitts operate in these two distinct regimes prior to coupling.

We define $\kappa_{12}$, the coupling strength from the OEO to Colpitts, as the ratio between the average photocurrent induced by the optical power incident on the PD2 and the average base current of the Colpitts oscillator before coupling. We define $\kappa_{21}$, the coupling strength from Colpitts to OEO, as the ratio between the injected average voltage from the Colpitts oscillator and the intrinsic average voltage of the OEO before coupling.

## III. PHASE SYNCHRONIZATION

In this section, the value of the various parameters that control the behavior of the OEO and the Colpitts oscillator are chosen such that, before coupling, both oscillators oscillate periodically. These values are listed in Table I.

Figure 2 shows the wave forms and the spectrum generated by the OEO and Colpitts under test, when the two oscillators are decoupled ($\kappa_{12} = \kappa_{21} = 0$) and both oscillate periodically. The intrinsic oscillation frequencies of the OEO ($f_{\mathrm{OEO-i}}$) and the Colpitts oscillator ($f_{\mathrm{Col-i}}$) are 296.87 and 304.15 kHz, respectively. The difference between these frequencies are selected such that synchronization can be achieved with accessible coupling strengths. As evident from the plots, OEO's output carries more noise and the output of Colpitts has a DC voltage shift of $+2$ V.

The behavior of the coupled oscillatory system is characterized by monitoring the oscillation frequency of each oscillator as the unidirectional coupling coefficients ($\kappa_{12}$ and $\kappa_{21}$) are changed. Figure 3(a) shows the oscillation frequency of OEO ($f_{\mathrm{OEO}}$) and Colpitts ($f_{\mathrm{Col}}$) plotted against $\kappa_{21}$ for different values of $\kappa_{12}$. The solid dots are the measured values of $f_{\mathrm{OEO}}$ while hollow squares are the measured values of $f_{\mathrm{Col}}$. $\kappa_{21}$ is varied between 0 and 0.014 while $\kappa_{12}$ is varied between 0 and 0.172. These ranges are selected such that the transitions between asynchronous and synchronous oscillations can be captured. For each value of $\kappa_{12}$, as $\kappa_{21}$ increases, $f_{\mathrm{OEO}}$ and $f_{\mathrm{Col}}$ are pulled toward each other until at a certain value of $\kappa_{21}$ they collapse into one single value that gradually grows by further increasing $\kappa_{21}$.

In Fig. 3(a) the trace of the black dots and black squares show that when $\kappa_{12} = 0$, $f_{\mathrm{OEO}}$ (black dots) is unidirectionally

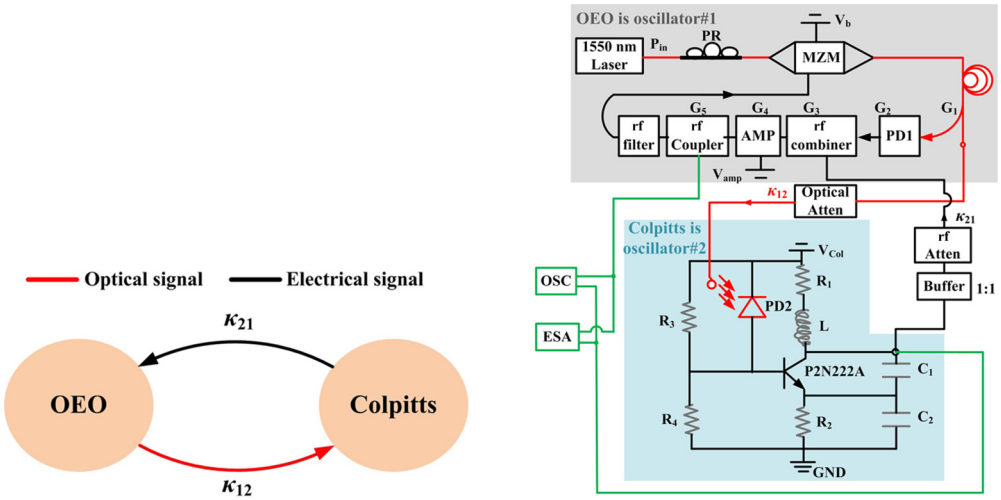


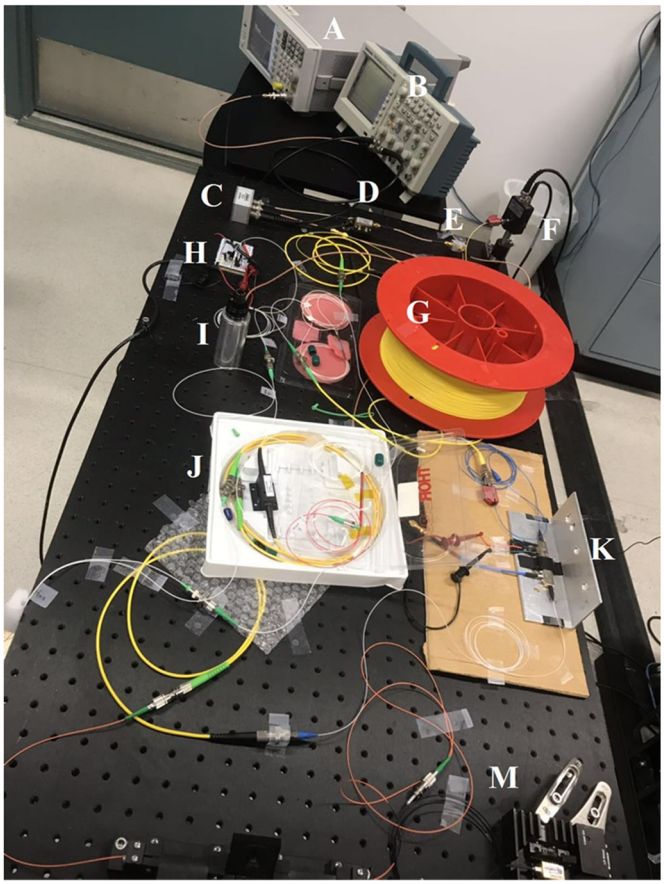


FIG. 1. (a) Schematic of the bidirectionally coupled OEO and Colpitts oscillator, the OEO is coupled to the Colpitts oscillator through optical power while the Colpitts oscillator is coupled to the OEO through voltage. $\kappa_{12}$ and $\kappa_{21}$ are the coupling strengths. (b) Circuit diagram for the bidirectionally coupled OEO and Colpitts oscillator used in the experiment. The circuits in green are the multichannel oscilloscope (OSC) and the electrical spectrum analyzer (ESA) for the wave and frequency spectrum monitoring. Here, $P_{\text{in}}$ is optical pump power of the OEO, $V_{\text{b}}$ is the DC bias voltage of the Mach-Zehnder modulator (MZM), $G_1$ is the coupling loss of the fiber coupler, $G_2$ is the voltage gain of the photodiode (PD1), $G_3$ is the voltage loss of the rf combiner, $G_4$ is the voltage gain of the rf amplifier, $G_5$ is the voltage loss of the rf coupler, $V_{\text{col}}$ is the drive voltage of the Colpitts oscillator, $L$ is the inductor, $R_1$, $R_2$, $R_3$, and $R_4$ are the resistors, $C_1$, $C_2$ are the capacitors, the transistor is P2N222A NPN transistor, and a photodiode (PD2) is biased between the voltage supply and the base port of the transistor with the responsivity as $\beta$. (c) The experimental setup that includes A: ESA; B: OSC; C: rf coupler; D: AMP; E: rf combiner; F: PD1; G: fiber delay; H: the PCB board contains Colpitts oscillator, buffer, and PD2; I: rf attenuator; J: optical attenuator; K: MZM; and M: laser.

TABLE I. Parameters for the OEO and Colpitts for them to oscillate periodically when they are uncoupled.

| Parameter | $P_{in}$ ($\mu$W) | $V_b$ (V) | $G_1$ | $G_2$ (V/W) | $G_3$ | $G_4$ |
|---|---|---|---|---|---|---|
| Value | 53.3 | 3.2 | 0.5 | 22670 | 0.5 | 57 |
| Parameter | $G_5$ | $V_{amp}$ (V) | $V_{col}$ (V) | $L$ ($\mu$H) | $R_1$ ($\Omega$) | $R_2$ ($\Omega$) |
| Value | 0.92 | 9 | 3 | 22 | 60.56 | 88.93 |
| Parameter | $R_3$ ($\Omega$) | $R_4$ ($\Omega$) | $C_1$ ($\mu$H) | $C_2$ ($\mu$H) | $\beta$ (A/W) | |
| Value | 75.90 | 300.6 | 29 | 39 | 0.96 | |

pulled up toward $f_{Col-i}$ as $\kappa_{21}$ increases, and at $\kappa_{21} = 0.006\,12$ collapses to $f_{Col-i}$. Here the sudden rise of $f_{OEO}$ from $\kappa_{21} = 0.005\,46$ to $\kappa_{21} = 0.006\,12$ is artificially induced by the resolution of the $\kappa_{21}$ variable while performing the measurement (due to the 1-dB attenuation step of the rf power attenuator used here). Similarly, the trace of the hollow squares with different colors on the $y$ axis, where $\kappa_{21} = 0$, shows $f_{Col}$ is unidirectionally pulled down toward $f_{OEO-i}$ as $\kappa_{12}$ increases, and collapses to $f_{OEO-i}$ at $\kappa_{12} = 0.172$. When both $\kappa_{12}$ and $\kappa_{21}$ are larger than zero, $f_{OEO}$ and $f_{Col}$ are pulled toward each other and collapse to a single oscillation frequency $f_s$ between the $f_{OEO-i}$ and $f_{Col-i}$ (i.e., the intrinsic oscillation frequencies of OEO and Colpitts) at a particular value of $\kappa_{12}$ for a given value of $\kappa_{21}$. The synchronization process can be visualized by plotting the frequency difference between the OEO and Colpitts ($\Delta f = f_{Col} - f_{OEO}$). Figure 3(b) shows $\Delta f$ plotted versus $\kappa_{21}$ for different values of $\kappa_{12}$. We see that $\Delta f$ is a monotonically decreasing function of both coupling strengths and becomes zero at particular values of $\kappa_{12}$ and $\kappa_{21}$ referred to as critical values ($\kappa_{12,C}$ and $\kappa_{21,C}$). The black dashed line in Fig. 3(a) shows a near linear relation between $f_s$ and $\kappa_{21,C}$.

Since each $\kappa_{21,C}$ is associated with a unique $\kappa_{12,C}$, a functional relation can be found between these critical values in the form $\kappa_{21,C} = F(\kappa_{12,C})$ or $\kappa_{12,C} = F^{-1}(\kappa_{21,C})$. Figure 3(c) shows the measured values of $\kappa_{12,C}$ plotted against $\kappa_{21,C}$. A match between measured data points and a linear fit reveals an approximately linear relationship between $\kappa_{21,C}$ and $\kappa_{12,C}$ in the form $\kappa_{12,C} + 26.837\kappa_{21,C} = 0.1675$. This means that the $\kappa_{21}$ is 26.837 times more *effective* than $\kappa_{12}$ in pulling the oscillation frequencies toward each other. In other words, one may define an equivalent coupling strength $\kappa_{eq} = \kappa_{12,C} + 26.837\kappa_{21,C}$ for this coupled oscillatory system where $\kappa_{eq} \geqslant 0.1675$ is the required condition for $\Delta f = f_{OEO} - f_{Col}$ to be zero. As shown in Fig. 2(b), the phase noise of OEO is larger

TABLE II. Parameters for the OEO and Colpitts corresponding to chaotic oscillations when they are uncoupled.

| Parameter | $P_{in}$ ($\mu$W) | $V_b$ (V) | $G_1$ | $G_2$ (V/W) | $G_3$ | $G_4$ |
|---|---|---|---|---|---|---|
| Value | 224.2 | 3.2 | 0.5 | 22670 | 0.5 | 57 |
| Parameter | $G_5$ | $V_{amp}$ (V) | $V_{col}$ (V) | $L$ ($\mu$H) | $R_1$ ($\Omega$) | $R_2$ ($\Omega$) |
| Value | 0.92 | 9 | 5 | 95 | 20.67 | 387 |
| Parameter | $R_3$ ($\Omega$) | $R_4$ ($\Omega$) | $C_1$ ($\mu$H) | $C_2$ ($\mu$H) | $\beta$ (A/W) | |
| Value | 65.30 | 183.57 | 50.8 | 50.8 | 0.96 | |

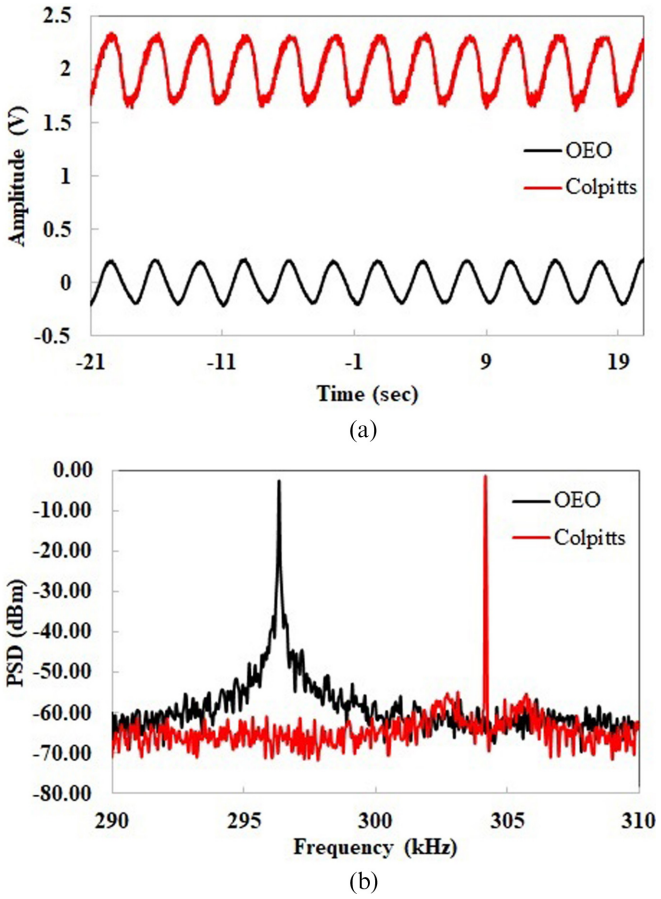


FIG. 2. (a) Wave forms generated by isolated OEO (black) and Colpitts oscillator (red). (b) Measured rf spectrum of isolated OEO (black) and Colpitts oscillator (red). Here $\kappa_{12} = \kappa_{21} = 0$.

than the phase noise of Colpitts; the quality factor of the OEO ($Q_1$) is smaller than the quality factor of Colpitts ($Q_2$) [41,42]. Generally for mutually coupled oscillators according to *Adler* model (or *Kuramoto* model), the pulling strength of the target oscillator is proportional to the ratio between the coupling strength ($\kappa_{ij}$) and the quality factor of the resonator (energy storage tank) of target oscillator [43–45]; this means the oscillator with higher quality factor is more resistive to be pulled, so in our system Colpitts (Osc 2) is more difficult to be pulled compared to the OEO (Osc 1) because $Q_2 > Q_1$—this may explain the lower efficiency of $\kappa_{12}$ compared to $\kappa_{21}$ in pulling the oscillation frequencies. Here we use the phase model (*Adler* model or *Kuramoto* model) derived based on coupled homogeneous oscillators to explain the efficiency of $\kappa_{12}$ and $\kappa_{21}$ for our coupled heterogeneous oscillators. While deriving a clear relation between the two coupling coefficients needs extensive study of two mutually coupled heterogeneous oscillators, derivation of a phase model for the coupled heterogeneous oscillator is much easier and yet helpful for studying the relation between the coupling coefficients.

While $\Delta f = 0$ is usually an indication of synchronized oscillation (in the context of injection locking), in order to better characterize synchronization we have also measured the phase difference between OEO and Colpitts. Figure 4 shows the variation of the measured phase difference between

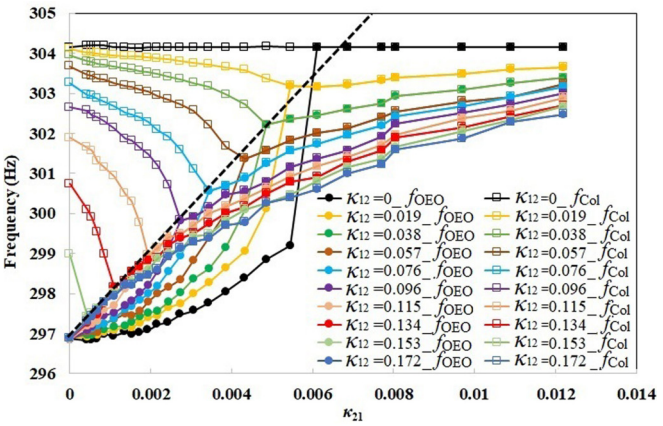

(a)

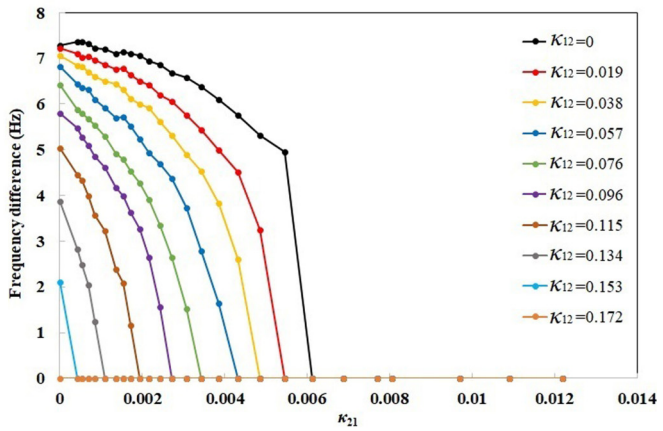

(b)

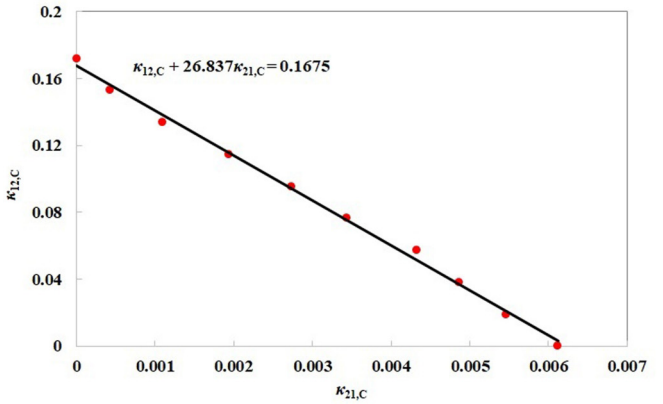

(c)

FIG. 3. Route to phase synchronization in the coupled OEO and the Colpitts oscillator. (a) Frequency of the OEO and Colpitts oscillator vs coupling strengths ($\kappa_{12}$, $\kappa_{21}$), (b) the frequency difference $\Delta f (= f_{Col} - f_{OEO})$ vs coupling strengths, and (c) the relation between the two coupling strengths ($\kappa_{12}$, $\kappa_{21}$) when the coupled OEO and Colpitts oscillator are just synchronized, the solid line is the linear fit of the data points.

the synchronized OEO and Colpitts oscillator ($\varphi_{Col} - \varphi_{OEO}$) as the coupling strengths are changed. The positive phase difference indicates that the Colpitts oscillator is leading the OEO. As shown in Fig. 4, the phase difference rises both by increasing $\kappa_{12}$ and increasing $\kappa_{21}$.

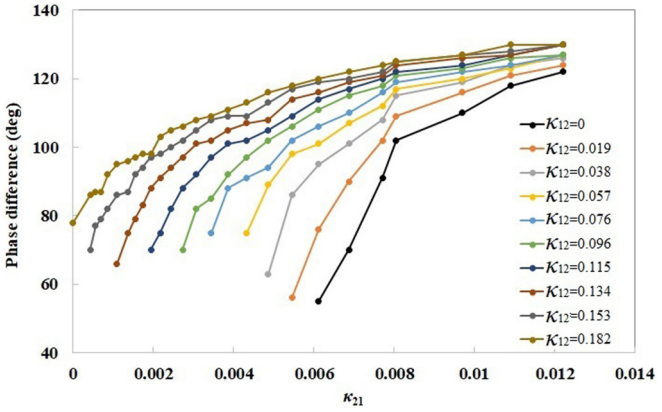


FIG. 4. The measured phase difference ($\varphi_{Col} - \varphi_{OEO}$) between the synchronized OEO and Colpitts oscillator plotted against $\kappa_{21}$ at different values of $\kappa_{12}$.

## IV. GENERALIZED CHAOS SYNCHRONIZATION

In this section, the control parameters of the OEO and the Colpitts oscillator are chosen such that they both oscillate chaotically before coupling. The values of these parameters are listed in Table II.

Figure 5(a) shows the measured wave forms generated by the chaotic OEO and the chaotic Colpitts oscillator when they are isolated ($\kappa_{12} = \kappa_{21} = 0$) and Fig. 5(b) shows their measured frequency spectra. The gray trace in Fig. 5(b) is the measured background noise of the electrical spectrum analyzer in the absence of an input. The black and red traces are the measured spectra for the OEO and the Colpitts oscillator, respectively. The measured spectrum for each oscillator comprises a few sharp peaks superimposed on a broad background; such combination of features in the power spectrum of an oscillator is typically considered as a signature of chaotic oscillation [46–48]. Using the measured wave forms, we have extracted the two largest Lyapunov exponents (LEs) for the OEO and the Colpitts oscillator. The Lyapunov exponents are $LE_{1,OEO} = 1.36 \times 10^6$ bit/sec, $LE_{2,OEO} = 2.90 \times 10^5$ bit/sec for the OEO, and $LE_{1,Col} = 8.41 \times 10^4$ bit/sec, $LE_{2,Col} = -1.39 \times 10^5$ bit/sec for the Colpitts oscillator [49]. The largest LE for the OEO is almost twenty times larger than the largest LE for the Colpitts oscillator; this difference is in agreement with the measured spectrum in Fig. 5(b) where the OEO's spectrum is extended to much larger frequencies compared to that of the Colpitts oscillator. The fact that the two largest LEs of the OEO are both positive indicates that the OEO is hyperchaotic. The fact that the largest LE of the Colpitts is positive while the second largest LE is negative indicates that the Colpitts oscillator is chaotic but not hyperchaotic [50].

Next, in order to investigate the emergence of synchronization as a function of the coupling strengths, the two oscillators are mutually coupled and the coupling strengths ($\kappa_{12}$ and $\kappa_{21}$) are increased. Generally, one can characterize synchronization using two standard techniques, namely, correlation function and the generalized return plots [51,52]. We introduce the correlation function $S(\Delta t)$ between two time-varying parameters

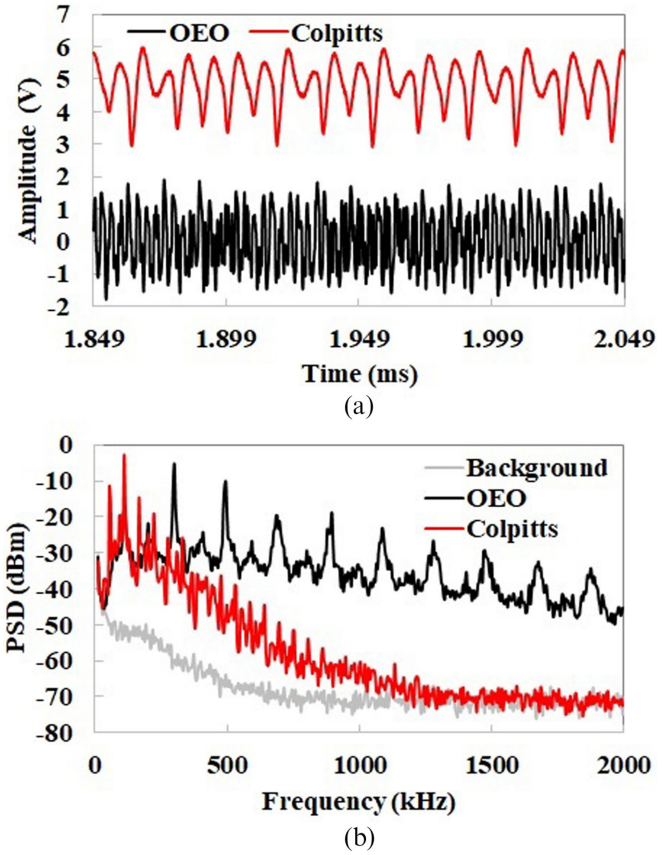


FIG. 5. (a) Measured wave form of the OEO (black) and the Colpitts oscillator (red), and (b) measured frequency spectrum of the OEO (black) and the Colpitts oscillator (red) when they are uncoupled ($\kappa_{12} = \kappa_{21} = 0$). The gray line in (b) is associated with the background noise of the ESA used for these measurements (when there is no input to the ESA).

$x_1(t)$ and $x_2(t)$ as

$$S(\Delta t) = \frac{\langle x_1(t)x_2(t-\Delta t)\rangle}{\sqrt{\langle x_1^2(t)\rangle\langle x_2^2(t)\rangle}}, \tag{1}$$

where $\langle\bullet\rangle$ indicates a time average over an extended period of time; here $x_1(t)$ is the OEO output voltage subtracted by its mean value $[x_1(t) = V_{\mathrm{OEO}}(t) - \overline{V_{\mathrm{OEO}}}]$ and $x_2(t)$ is the Colpitts output voltage subtracted by its mean value $[x_2(t) = V_{\mathrm{Col}}(t)–\overline{V_{\mathrm{Col}}}]$. We search for the time shift $\Delta t$ at which the correlation between the outputs of OEO and Colpitts is maximized. The maximum value of $S$ is typically referred to as correlation degree.

Figure 6 shows the correlation degree $[\max\{S(\Delta t)\}]$ calculated at different coupling strengths ($\kappa_{12}$, $\kappa_{21}$) that happened at a certain time shift $\Delta t$. Figure 6(a) plots the correlation degree versus coupling strengths, while Fig. 6(b) plots the corresponding time shift for the correlation degrees in Fig. 6(a). We can see, as the coupling strengths increase, the correlation degree increases rapidly from 0.1 (when $\kappa_{12} = \kappa_{21} = 0$) until it reaches a saturation value ~0.8 (when $\kappa_{12} > 0.53$ and $\kappa_{21} > 0.04$). Note that, while for two isolated oscillators, the correlation degree should be zero, the experimentally measured signal has a correlation degree of $\max(S) = 0.1$ when

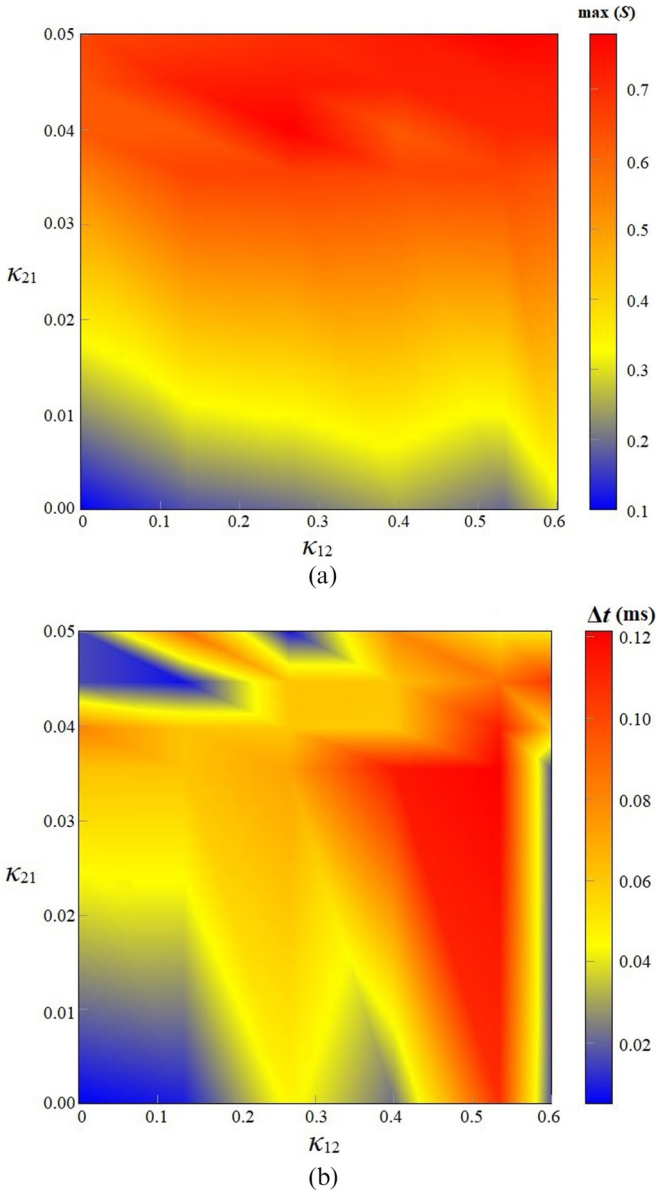


FIG. 6. (a) Correlation degree $[\max\{S(\Delta t)\}]$ calculated for different values of $\kappa_{12}$ and $\kappa_{21}$ that occur at (b) certain time shift $\Delta t$.

$\kappa_{12} = \kappa_{21} = 0$. It is believed that this is due to unwanted coupling through electromagnetic radiation and antenna effects associated with wires, and other electrical components used in the experimental setup.

The large correlation (~0.8) between the outputs of the OEO and the Colpitts oscillator at large coupling strengths indicates the two oscillators are essentially synchronized [51]. To further investigate the onset of synchronization between these originally chaotic oscillators, in Fig. 7 $S(\Delta t)$ is plotted versus $\Delta t$ (time shift) when $\kappa_{12} = \kappa_{21} = 0$ and when $\kappa_{12} = 0.6008$, $\kappa_{21} = 0.0501$. As mentioned before, the weak correlation shown in Fig. 7(a) is due to the parasitic electromagnetic coupling. Figure 7(b) shows the appearance of sharp peaks at $\Delta t = n \times \tau$ ($n = 1, 2, 3, \ldots$) where $\tau \sim 0.0073$ ms.

The largest peak of $S(\Delta t)$ [marked by a red dot in Fig. 7(b)] indicates synchronized chaotic oscillation.

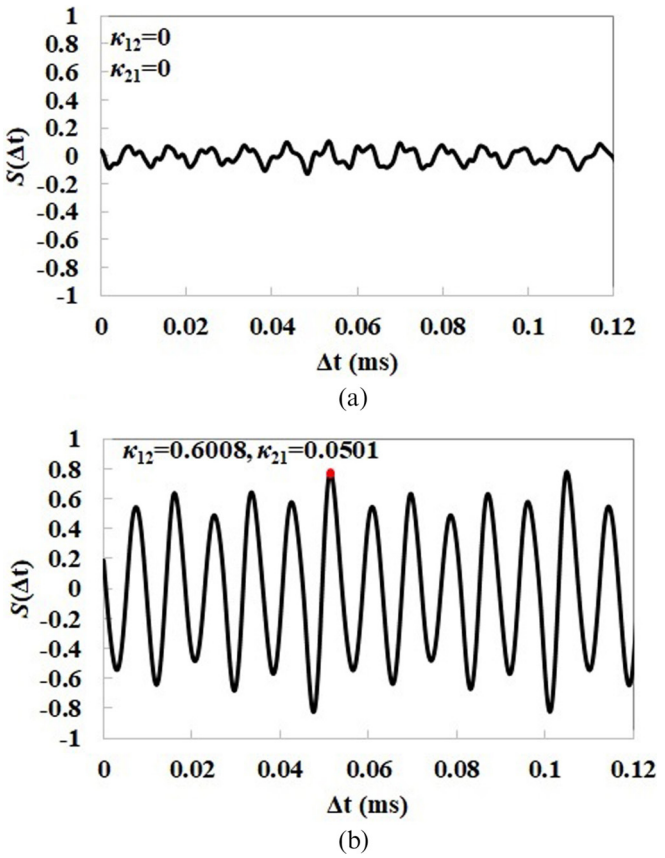


FIG. 7. Correlation function for coupled OEO and Colpitts oscillator (both operating in chaotic regime) when (a) $\kappa_{12} = \kappa_{21} = 0$ and (b) $\kappa_{12} = 0.6008$, $\kappa_{21} = 0.0501$.

This peak has a magnitude of 0.77 and it appears at $\Delta t = 0.051$ ms.

We also calculated the similarity function for $x_1(t)$ and $x_2(t - \Delta t)$ when $\kappa_{12} = 0.6008$, $\kappa_{21} = 0.0501$ defined as

$$Dist[x_1(t), x_2(t - \Delta t)] = \sqrt{\sum_t |x_1(t) - x_2(t - \Delta t)|^2}. \quad (2)$$

Figure 8 shows the calculated similarity function based on measured values of $x_1(t)$ and $x_2(t)$ at different time delays ($\Delta t$). As expected from Fig. 7, the similarity function has a local minimum at $\Delta t = 0.051$ ms (where the correlation function is maximum), at which the two chaotic oscillators oscillate in synchrony.

The temporal variation of the corresponding output signals (when $\kappa_{12} = 0.6008$, $\kappa_{21} = 0.0501$) is shown in Fig. 9(a). Figure 9(b) shows $x_1(t)$ and $x_2(t - 0.05\,\text{ms})$. The overlap and coincidence of the maxima and minima of one wave form with a time shifted version of the other wave form observed here is known as achronal generalized synchronization [13,52]. Figure 9(c) shows a generalized return plot where $x_1(t)$ is plotted against $x_2(t - 0.05\,\text{ms})$. As evident from the plot the oscillation amplitudes are confined within a narrow region that is extended approximately along a 45° direction. The dynamical properties of this achronal state originate from the bidirectional coupling of the two physically dissimilar subsystems. It is worth noting that the achronal state is not

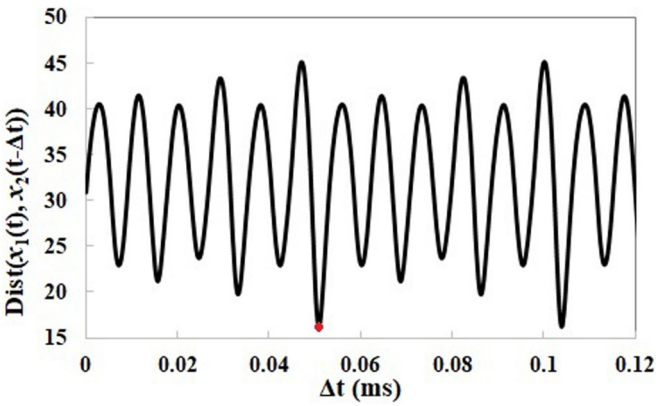


FIG. 8. Similarity function calculated for coupled oscillatory system comprising of mutually coupled OEO and Colpitts oscillators where both oscillators operate in chaotic regime. The similarity function is calculated based on measured values of $x_1(t)$ and $x_2(t)$, when $\kappa_{12} = 0.6008$, $\kappa_{21} = 0.0501$.

a perfectly synchronized state of the coupled system; such a state may only exist for coupled periodic oscillators [51,52]. The spectrum of the coupled chaotic system under generalized synchronization is shown in Fig. 9(d), which still consists of a broad spectrum with many sharp peaks.

When the OEO and Colpitts oscillator are synchronized (for $\kappa_{12} = 0.6008$, $\kappa_{21} = 0.0501$), we measured the two largest LEs for the system with $LE_1 = 2.28 \times 10^5$ bit/sec and $LE_2 = -1.55 \times 10^5$ bit/sec. Both the spectrum and the LEs indicate that the system is chaotic.

We have calculated the two largest LEs for the coupled system based on the signal measured through the rf coupler in OEO loop [see Fig. 1(b)] at different values of $\kappa_{12}$ and $\kappa_{21}$. We have found that as the coupling strengths increase, the system transitions from hyperchaos to chaos. For example, when $\kappa_{12} = 0.1335$ and $\kappa_{21} = 0.0355$, the two largest LEs of the system are $LE_1 = 4.98 \times 10^5$ bit/sec and $LE_2 = 8.80 \times 10^4$ bit/sec, indicating the system is in hyperchaotic regime. When the $\kappa_{12} = 0.6008$ and $\kappa_{21} = 0.0501$ [with the attractor shown in Fig. 9(c)], the system becomes chaotic with the two largest LEs measured as $LE_1 = 2.28 \times 10^5$ bit/sec and $LE_2 = -1.44 \times 10^5$ bit/sec.

Figures 10(a) and 10(b) show the largest and the second largest LE of the coupled system as a function of $\kappa_{12}$ and $\kappa_{21}$ respectively. As evident from the plots, the largest LE [Fig. 10(a)] decreases from $1.36 \times 10^6$ bit/sec when $\kappa_{12} = \kappa_{21} = 0$ to $2.28 \times 10^5$ bit/sec when $\kappa_{12} = 0.6008$ and $\kappa_{21} = 0.0501$, while the second largest LE [Fig. 10(b)] decreases from $2.90 \times 10^5$ bit/sec when $\kappa_{12} = \kappa_{21} = 0$ to $-1.55 \times 10^5$ bit/sec when $\kappa_{12} = 0.6008$ and $\kappa_{21} = 0.0501$. Additionally, Fig. 10(b) shows a gradual transition of the second largest LE from positive to negative values in a certain region of $\kappa_{12} - \kappa_{21}$ plane indicating a gradual transition from hyperchaos to chaos.

## V. CONCLUSION

We have experimentally studied the behavior of a coupled oscillatory system comprising two physically dissimilar oscillators coupled bidirectionally through two different cou-

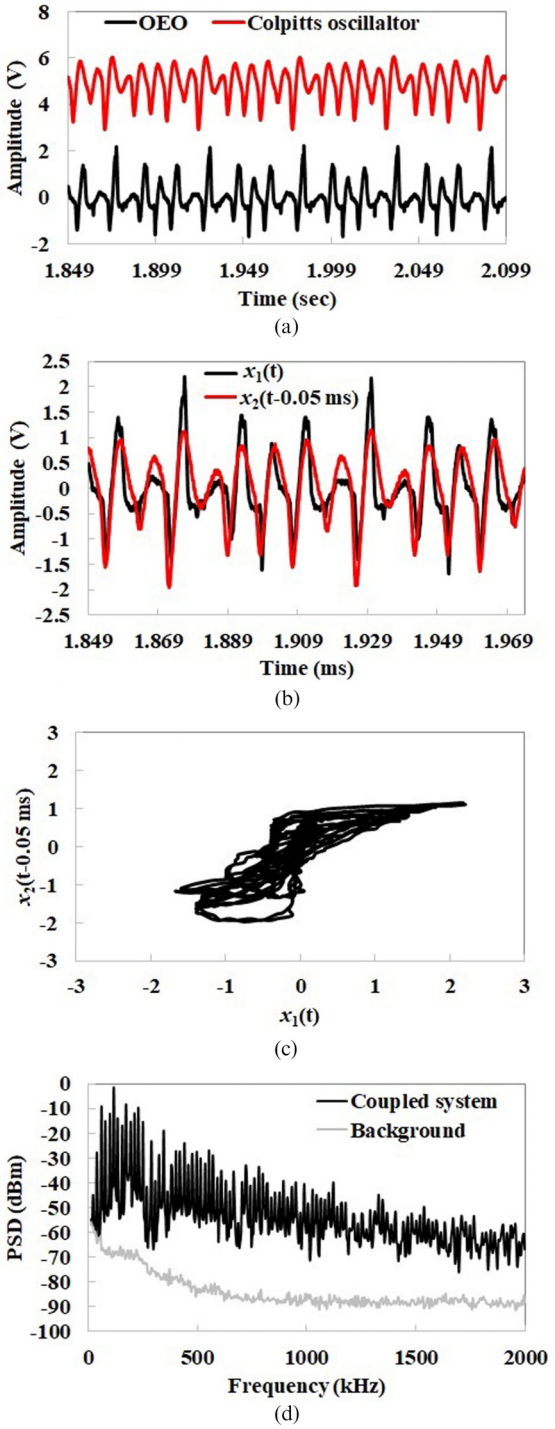


FIG. 9. Characterization of output signals generated by the synchronized OEO and Colpitts oscillator when both oscillators are operating in chaotic regime, here $\kappa_{12} = 0.6008$ and $\kappa_{21} = 0.0501$. (a) The output wave form extracted from the OEO (black) and Colpitts oscillator (red). (b) The time trace of $x_1(t)$ and $x_2(t - 0.05\,\text{ms})$. (c) The generalized return plot for of $x_1(t)$ and $x_2(t - 0.05\,\text{ms})$. (d) The frequency spectrum of the OEO measured through the output port of the rf coupler in the OEO loop shown in Fig. 1(b). The gray line in (d) is the background noise spectrum of the ESA (in the absence of input). Here $x_1(t)$ is the output wave form of OEO subtracted with its mean value and $x_2(t - 0.05\,\text{ms})$ is the output wave form of the Colpitts oscillator subtracted with its mean value and then shifted with a time of 0.05 ms.

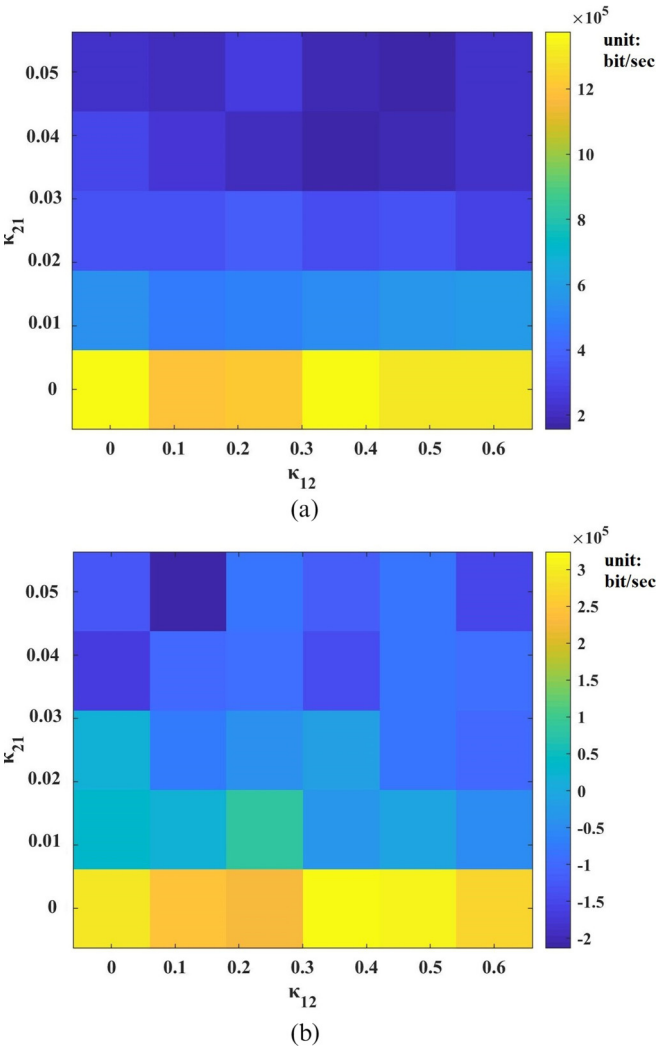


FIG. 10. Variation of the two largest Lyapunov exponents (LEs) of the measured OEO output as a function of coupling strengths ($\kappa_{12}$ and $\kappa_{21}$). (a) Contour plot of the largest LE. (b) Contour plot of the second largest LE.

pling mechanisms. More specifically we have characterized the behavior of a coupled system wherein an optoelectronic oscillator (OEO) is coupled to a Colpitts oscillator (an electronic oscillator) via optical power, and the Colpitts is coupled back to the OEO via rf voltage. The output signals from both oscillators were measured and characterized for two different parameter sets and at different coupling strengths. First the parameters of both oscillators were adjusted such that, before coupling, they oscillate periodically at slightly different frequencies. In the resulting coupled system, we observed transition from independent oscillation to synchronized oscillation at critical values of the two coupling strengths. Interestingly we found that these critical values are linearly related. Next, the parameters of both oscillators were adjusted such that, before coupling, they both oscillate chaotically. In this case for certain values of coupling strength we observed generalized chaos synchronization upon coupling the two oscillators. In this system we also observed a transition from hyperchaos to chaos in a specific coupling regime.

The experimental arrangement, selected coupling mechanisms, measurement strategy, and the results obtained in this paper may pave the way toward designing new experiments that enable characterizing coupled systems that involve coupling between a larger variety and larger number of oscillators. Understanding the complex dynamics of such highly heterogeneous systems is critical for many disciplines of science and engineering.

The data that support the findings of this study are available from the corresponding author upon reasonable request.

## ACKNOWLEDGMENT

This study was supported by the National Science Foundation (NSF) under Grant No. 1727948.

[1] M. Dolnik and I. R. Epstein, Coupled chaotic chemical oscillators, Phys. Rev. E **54**, 3361 (1996).

[2] B. Blasius, E. Montbrio, and J. Kurths, Anomalous phase synchronization in populations of nonidentical oscillators, Phys. Rev. E **67**, 035204(R) (2003).

[3] P. Woafo and H. G. Enjieu Kadji, Synchronized states in a ring of mutually coupled self-sustained electrical oscillators, Phys. Rev. E **69**, 046206 (2004).

[4] D. M. Abrams and S. H. Strogatz, Chimera States for Coupled Oscillators, Phys. Rev. Lett. **93**, 174102 (2004).

[5] O. V. Popovych, S. Yanchuk, and P. A. Tass, Delay- and Coupling-Induced Firing Patterns in Oscillatory Neural Loops, Phys. Rev. Lett. **107**, 228102 (2011).

[6] A. Xuereb, C. Genes, and A. Dantan, Strong Coupling and Long-Range Collective Interactions in Optomechanical Arrays, Phys. Rev. Lett. **109**, 223601 (2012).

[7] K. M. Hannay, D. B. Forger, and V. Booth, Macroscopic models for networks of coupled biological oscillators, Sci. Adv. **4**, e1701047 (2018).

[8] L. J. Pei, L. X. Duan, and H. Y. Liu, Dynamics of the Coupled Lorenz-Rössler Systems, in *International Workshop on Chaos-Fractal Theories and Applications* (IEEE, China, 2010), p. 271.

[9] P. K. Roy, C. Hens, I. Grosu, and S. K. Dana, Engineering generalized synchronization in chaotic oscillators, Chaos **21**, 013106 (2011).

[10] G. Tanaka, K. Morino, H. Daido, and K. Aihara, Dynamical robustness of coupled heterogeneous oscillators, Phys. Rev. E **89**, 052906 (2014).

[11] M. R. Guevara, L. Glass, and A. Shrier, Phase-locking, period-doubling bifurcations and irregular dynamics in periodically stimulated cardiac cells, Science **214**, 1350 (1981).

[12] R. Roy and K. S. Thornburg, Experimental Synchronization of Chaotic Lasers, Phys. Rev. Lett. **72**, 2009 (1994).

[13] T. Heil, I. Fischer, and W. Elsässer, J. Mulet, and C. R. Mirasso, Chaos Synchronization and Spontaneous Symmetry-Breaking in Symmetrically Delay-Coupled Semiconductor Lasers, Phys. Rev. Lett. **86**, 795 (2001).

[14] H. D. I. Abarbanel, N. F. Rulkov, and M. M. Sushchik, Generalized synchronization of chaos: The auxiliary system approach, Phys. Rev. E **53**, 4528 (1996).

[15] R. Banerjee, D. Ghosh, E. Padmanaban, R. Ramaswamy, L. M. Pecora, and S. K. Dana, Enhancing synchrony in chaotic oscillators by dynamic relaying, Phys. Rev. E **85**, 027201 (2012).

[16] K. A. Blaha, K. Huang, F. D. Rossa, L. Pecora, M. Hossein-Zadeh, and F. Sorrentino, Cluster Synchronization in Multilayer Networks: A Fully Analog Experiment with LC Oscillators with Physically Dissimilar Coupling, Phys. Rev. Lett. **122**, 014101 (2019).

[17] G. Heinrich, M. Ludwig, J. Qian, B. Kubala, and F. Marquardt, Collective Dynamics in Optomechanical Arrays, Phys. Rev. Lett. **107**, 043603 (2011).

[18] M. R. Tinsley, S. Nkomo, and K. Showalter, Chimera and phase-cluster states in populations of coupled chemical oscillators, Nat. Phys. **8**, 662 (2012).

[19] M. Bagheri, M. Poot, L. R. Fan, F. Marquardt, and H. X. Tang, Photonic Cavity Synchronization of Nanomechanical Oscillators, Phys. Rev. Lett. **111**, 213902 (2013).

[20] C. R. S. Williams, T. E. Murphy, R. Roy, F. Sorrentino, T. Dahms, and E. Scholl, Experimental Observations of Group Synchrony in a System of Chaotic Optoelectronic Oscillators, Phys. Rev. Lett. **110**, 064104 (2013).

[21] C. R. S. Williams, F. Sorrentino, T. E. Murphy, and R. Roy, Synchronization states and multistability in a ring of periodic oscillators: Experimentally variable coupling delays, Chaos **23**, 043117 (2013).

[22] C. Schäfer, M. G. Rosenblum, J. Kurths, and H. H. Abel, Heartbeat synchronized with ventilation, Nature (London) **392**, 239 (1998).

[23] I. Ozden, S. Venkataramani, M. A. Long, B. W. Connors, and A. V. Nurmikko, Strong Coupling of Nonlinear Electronic and Biological Oscillators: Reaching the Amplitude Death Regime, Phys. Rev. Lett. **93**, 158102 (2004).

[24] C. Droin, E. R. Paquet, and F. Naef, Low-dimensional dynamics of two coupled biological oscillators, Nat. Phys. **15**, 1086 (2019).

[25] A. Pikovsky, M. Rosenblum, and J. Kurths, Synchronization, in *A Universal Concept in Nonlinear Sciences* (Cambridge University Press, Cambridge, UK, 2001), chap. 6.

[26] A. B. Dubois, A. W. Brody, D. H. Lewis, and B. F. Burgess, Oscillation mechanics of lungs and chest in man, J. Appl. Physiol. **8**, 587 (1956).

[27] A. J. Connolly, W. E. Finkbeiner, P. C. Ursell, and R. L. Davis, in *Microscopic Examination* (Elsevier, New York, 2016), Chap. 8.

[28] Y. Lan, Z. Q. Liu, H. M Zhang, X. L. Ding, M. H. Yang, H. G. Gu, and W. Ren, Noise-induced synchronous stochastic oscillations in small scale cultured heart-cell networks, Chin. Phys. B **20**, 020508 (2011).

[29] C. Foerch, H. W. Korf, H. Steinmetz, M. Sitzer, and A. S. Hessen, Abrupt shift of the pattern of diurnal variation in stroke onset with daylight saving time transitions, Circulation **118**, 284 (2008).

[30] P. Franco, D. Verheulpen, F. Valente, I. Kelmanson, Alainde Broca, S. Scaillet, J. Groswasser, and A. Kahn. Autonomic responses to sighs in healthy infants and in victims of sudden infant death, Sleep Med. **4**, 569 (2003).

[31] A. Prasad, S. K. Dana, R. Karnatak, J. Kurths, B. Blasius, and R. Ramaswamy, Universal occurrence of the phase-flip bifurcation in time-delay coupled systems, Chaos **18**, 023111 (2008).

[32] B. M. Adhikari, A. Prasad, and M. Dhamala, Time-delay-induced phase-transition to synchrony in coupled bursting neurons, Chaos **21**, 023116 (2011).

[33] Y. K. Chembo, L. Larger, H. Tavernier, R. Bendoula, E. Rubiola, and P. Colet, Dynamic instabilities of microwaves generated with optoelectronic oscillators, Opt. Lett. **32**, 2571 (2007).

[34] Y. K. Chembo, L. Larger, and P. Colet, Nonlinear dynamics and spectral stability of optoelectronic microwave oscillators, IEEE J. Quant. Electron. **44**, 858 (2008).

[35] M. Peil, M. Jacquot, Y. K. Chembo, L. Larger, and T. Erneux, Routes to chaos and multiple time scale dynamics in broadband bandpass nonlinear delay electro-optic oscillators, Phys. Rev. E **79**, 026208 (2009).

[36] K. E. Callan, L. Illing, Z. Gao, D. J. Gauthier, and E. Schöll, Broadband Chaos Generated by an Optoelectronic Oscillator, Phys. Rev. Lett. **104**, 113901 (2010).

[37] M. P. Kennedy, Chaos in the Colpitts oscillator, IEEE Trans. Circuits Syst. **41**, 771 (1994).

[38] O. D. Feo and G. M. Maggio, Bifurcations in the Colpitts oscillator: From theory to practice, Int. J. Bifurcation Chaos **13**, 2917 (2003).

[39] J. Kengne, J. C. Chedjou, G. Kenne, and K. Kyamakya, Dynamical properties and chaos synchronization of improved Colpitts oscillators, Commun. Nonlinear Sci. Numer. Simulat. **17**, 2914 (2012).

[40] L. K. Kana, A. Fomethe, H. B. Fotsin, E. T. Wembe, and A. I. Moukengue, Complex dynamics and synchronization in a system of magnetically coupled Colpitts oscillators, J. Nonlinear Dyn. **2017**, 5483956 (2017).

[41] D. B. Leeson, A simple model of feedback oscillator noise spectrum, Proc. IEEE **54**, 329 (1966).

[42] H. W. Chen, H. C. Lu, and T. W. Huang, The analysis of relation between Q-factor and phase noise by using substrate-integrated waveguide cavity oscillators, in *Noise-induced synchronous stochastic oscillations in small scale cultured heart-cell networks* (IEEE, China, 2005), p. 4.

[43] R. A. York, P. Liao, and J. J. Lynch, Oscillator array dynamics with broadband N-Port coupling networks, IEEE Trans. Microwave Theory Tech. **42**, 2040 (1994).

[44] B. Razavi, A study of injection locking and pulling in oscillators, IEEE J. Solid-State Circuits **39**, 1415 (2004).

[45] A. Mirzaei and H. Darabi, Mutual pulling between two oscillators, IEEE J. Solid-State Circuits **49**, 360 (2014).

[46] D. Farmer, J. Crutchfield, H. Frochling, N. Packard, and R. Shaw, Power spectra and mixing properties of strange attractors, in *International Conference on Nonlinear Dynamics* (New York, 1979), Vol. 357, pp. 453–472.

[47] R. S. Dumont and P. Brumer, Characteristics of power spectra for regular and chaotic systems, J. Chem. Phys. **88**, 1481 (1988).

[48] M. C. Valsakumar, S. V. M. Satyanarayana, and V. Sridhar, Signature of chaos in power spectrum, Pramana J. Phys. **48**, 69 (1997).

[49] M. Sano and Y. Sawada, Measurement of the Lyapunov Spectrum from a Chaotic Time Series, Phys. Rev. Lett. **55**, 1082 (1985).

[50] A. Čenys, A. Tamaševičius, A. Baziliauskas, R. Krivickas, and E. Lindberg, Hyperchaos in coupled Colpitts oscillators, Chaos, Solitons Fractals **17**, 349 (2003).

[51] J. Mulet, C. Mirasso, T. Heil, and I. Fischer, Synchronization scenario of two distant mutually coupled semiconductor lasers, J. Opt. B: Quantum Semiclass. Opt. **6**, 97 (2004).

[52] J. K. White, M. Matus, and J. V. Moloney, Achronal generalized synchronization in mutually coupled semiconductor lasers, Phys. Rev. E **65**, 036229 (2002).